spontaneously (bending force constant for the linear species is −0.0231 mdyn Å rad^{-2}), to give a slightly bent true minimum whose bond angle is 173.9° and bending frequency is 69 cm^{-1}. These results are inconsistent with those obtained here at the DZP/SCF level, for which the linear species is a true minimum, whose bending force constant of 0.240 mdyn Å rad^{-2} produces a bending frequency of 156 cm^{-1}. Our DZP results are similar to those obtained with larger basis sets (TZ2P and TZ2Pf bending frequencies are 185 and 189 cm^{-1}, respectively), so it seems clear that the DZP basis performs much more satisfactorily than does the 6-31G*. We doubt that the discrepancy is due to the choice of polarization exponent, as the 6-31G* value of 0.65 is not greatly different from that of 0.532 which we used in this work, but suggest that the constraint of equal s and p exponents made in the interest of computational efficiency may be responsible for the poor performance of the 6-31G* basis in this case. It is notable that the optimum s and p Slater exponents are indeed almost equal for first-row atoms such as oxygen (2.246 for 2s and 2.227 for 2p[39]) but rather different for sulfur (2.122 for 3s and 1.827 for 3p). The contracted nature of the 3s orbitals relative to 3p for second-row atoms has been highlighted by Kutzelnigg[40] and by BM.[7] It seems possible that this undesirable feature of the 6-31G* basis contributes to the discrepancies apparent in two recent theoretical studies of the structural isomerism of S_4; the 6-31G* basis was used in one case,[41] whereas DZP and TZ2P basis sets similar to those employed here were adopted in the other.[37]

A point of structural interest concerns the possible dimerization of two S_3^{2+} units to form S_6^{4+}, since Te_6^{4+} has been isolated and shown to adopt a trigonal prismatic structure (D_{3h} symmetry),[42] while Te_3^{2+} is as yet unknown. We believe that this possibility is most unlikely in the sulfur case, at least for S_3^{2+} as an isolated species. The geometry of S_6^{4+} (assumed to be a singlet, since the ready observation of an ordinary Te NMR spectrum[42] for Te_6^{4+} strongly suggests that it is a singlet) was optimized at the DZP/SCF level, under the constraint of D_{3h} symmetry. Within the triangular faces the distance is 2.037 Å, typical of an S–S single bond and almost identical with that found for **3**, but the distance between the trigonal faces of 2.775 Å indicates a weak interaction between them. No vibrational analysis was performed for S_6^{4+}, but its SCF energy is no less than 1317 kJ mol^{-1} higher than 2 mol of **2** (the lowest singlet state of S_3^{2+}), and at the MP3 level the energy separation is still 1278 kJ mol^{-1}. It is, however, conceivable that S_6^{4+} might be stabilized in the solid state by the high lattice energy which its 4+ charge would produce or that interactions with a highly polar solvent might be strong enough to favor S_6^{4+} over two S_3^{2+} molecules. The binding between the trigonal faces is evidently much stronger in Te_6^{4+} than in S_6^{4+}, since the distance in the Te compound between the triangular faces of 3.133 Å exceeds that within the faces by only 0.458 Å,[42] or 17%, a substantially smaller margin than the 0.738 Å (36%) found here for S_6^{4+} at the DZP/SCF level. "Secondary bonding", or association of small units into larger polymeric ones, is characteristic of atoms as heavy as Te.[43]

Acknowledgment. This research was supported by the U.S. National Science Foundation, Grant CHE-8718469. C.J.M. thanks Professor H. F. Schaefer and the other members of the CCQC for their hospitality and generosity during his stay, the Australian Research Council for financial support, and The University of Melbourne and Cray Research for generous allocations of time on Cyber 990 and Cray Y-MP computers, respectively.

(39) Clementi, E.; Raimondi, D. *J. Chem. Phys.* **1964**, *38*, 2868.
(40) Kutzelnigg, W. *Angew. Chem., Int. Ed. Engl.* **1984**, *23*, 272.
(41) Raghavachari, K.; Rohlfing, C.; Binkley, J. S. *J. Chem. Phys.* **1990**, *93*, 5862.
(42) Burns, R. C.; Gillespie, R. J.; Luk, W.-C.; Slim, D. R. *Inorg. Chem.* **1979**, *18*, 3086.
(43) Alcock, N. R. *Adv. Inorg. Chem. Radiochem.* **1972**, *15*, 2–58.

Polymorphism in the Heavier Analogues of the Ethyl Cation

Georges Trinquier

Contribution from the Laboratoire de Physique Quantique, C.N.R.S., U.R.A. n°505, Université Paul-Sabatier, 31062 Toulouse Cedex, France. *Received December 6, 1991*

Abstract: Exploration of the potential energy surfaces for $X_2H_5^+$ throughout group 14 is carried out through ab initio calculations. Besides to two forms well-documented for the ethyl cation, the classical form $H_3C–CH_2^+$, **1**, and the C_{2v} bridged nonclassical form, **2**, there exist two other possible isomers, corresponding to the adduct $XH_4 + XH^+$. One is singly bridged, $H_3X–H–XH^+$, **4**, and the other one is doubly bridged $H_2X<^{H}_{H}>XH^+$, **3**. These forms, close in energy and separated by small barriers, are found to be true minima in all surfaces except for $C_2H_5^+$. The doubly bridged form **3** happens to be the preferred isomer for $Sn_2H_5^+$ and $Pb_2H_5^+$. The nonclassical form **2** is only a saddle point for $Ge_2H_5^+$, $Sn_2H_5^+$, and $Pb_2H_5^+$. The existences and relative stabilities of the various forms can finally be estimated as follows: $C_2H_5^+$, **2**; $Si_2H_5^+$, **1** ≈ **2** < **3** < **4**; $Ge_2H_5^+$, **1** < **3** < **4**; $Sn_2H_5^+$ and $Pb_2H_5^+$, **3** < **4** < **1**. The minimum energy barriers for **1**–**3** intramolecular conversions are calculated at around 20 kcal/mol, which should support the coexistence of both isomers. The relative stabilities of **1** and **3** can be roughly predicted from the balance between the X–X σ bond energies and the almost constant energy increments required in the dissociation of the double bridges into two fragments. Such simple modelling should apply to any competition between and X–X σ bond and X–H–X bridges.

The gas-phase structure of the ethyl cation $C_2H_5^+$ is now well-established from theoretical studies. The most refined calculations show that there is only one minimum on the corresponding potential energy surface, namely the nonclassical singly bridged C_{2v} form, **2**.[1–4] The classical form $H_3C–CH_2^+$, **1**, which is found to be a real minimum at lowest levels of calculations, actually collapses into the bridged form as soon as correlation effects are properly taken into account. The classical form is thus only a saddle point in an intramolecular hydrogen scrambling

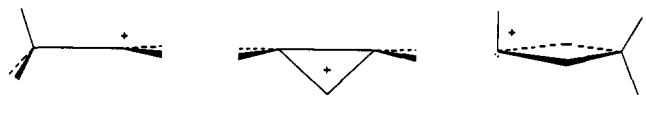

1 2 3

(1) Raghavachari, K.; Whiteside, R. A.; Pople, J. A.; Schleyer, P. v. R. *J. Am. Chem. Soc.* **1981**, *103*, 5649.
(2) Hehre, W. J.; Radom, L.; Schleyer, P. v. R.; Pople, J. A. *Ab initio Molecular Orbital Theory*; John Wiley and Sons: New York, 1986; p 384.
(3) Ruscic, B.; Berkowitz, J.; Curtiss, L. A.; Pople, J. A. *J. Chem. Phys.* **1989**, *91*, 114.
(4) Klopper, W.; Kutzelnigg, W. *J. Phys. Chem.* **1990**, *94*, 5625.

0002-7863/92/1514-6807$03.00/0

reaction. This theoretical description of the ethyl cation potential surface is in agreement with the photoionization mass spectrum of the ethyl radical.[3] Little is known about the heavier $X_2H_5^+$ analogues in group 14, except $Si_2H_5^+$ which has been the object of several theoretical studies.[5-7] All refined treatments on such a system indicate that both forms **1** and **2** are true minima with virtually the same energy. However, photoionization mass spectroscopic studies on the disilaethyl radical also suggest the existence of a third "state or structure" for $Si_2H_5^+$.[8] In a recent theoretical study of the $Si_2H_5^+$ potential surface, we confirmed the existence of a third minimum.[9] Such an isomer has a doubly bridged structure, **3**, which anticipates its natural dissociation into $SiH^+(^1\Sigma^+) + SiH_4$. In the meantime, Raghavachari found another minimum, also corresponding to an $SiH^+ + SiH_4$ adduct,[10] with a single bridge: $H_3Si-H-SiH^+$, **4**.

4

In the present work, we undertake the theoretical exploration, through ab initio calculations, of the potential surfaces for all group 14 $X_2H_5^+$ cations. The study will address the determination of all the stationary points, including the different possible isomers, the saddle points for intramolecular rearrangements, and the main dissociation products $XH_3^+ + XH_2(^1A_1)$, $XH^+(^1\Sigma^+) + XH_4$, and $X_2H_4 + H^+$.

The geometries are optimized at the SCF level using valence basis sets of DZP quality. The core electrons are taken into account through an effective core potential technique. For the tin and lead atoms these potentials take into account the mean relativistic effects. Further checks were occasionally made with CASSCF geometry optimization. On all the SCF-optimized geometries, MP4 calculations were performed to assess the effects of electron correlation on the energetics. All technical details are given in the Appendix.

Search for Stationary Points

For heavy-atom-containing molecules, many studies have established the preference for singly, doubly, or polybridged arrangements.[11-13] Such bridged structures will therefore be candidates for our isomers. To find them, the various ways the X_2H_4 forms can be protonated into $X_2H_5^+$ may be considered (Figure 1). Protonation of one extracyclic lone pair of a doubly bridged form as well as protonation of the shared lone pair of the singly bridged form both suggest the possible doubly bridged isomer **3** for the cation. This structure was found to be a real minimum for all the $X_2H_5^+$ cations except $C_2H_5^+$. For $C_2H_5^+$, such a C_s arrangement collapses into the eclipsed classical form, but it actually corresponds to a neat shouldering on the potential energy surface. A further polybridged arrangement, **5**, was explored for the heaviest cation $Pb_2H_5^+$. This D_{3h} triply bridged structure only corresponds to a critical point of index 3 on the potential surface.[14] The singly bridged structure **4** does not clearly emerge from this protonation scheme. This form may result from the opening of one bridge in **3** and owes much of its stability to the global positive charge that permits an electrostatically favored linear arrangement $X^+-H^--X^+$. This C_s structure was found to be a real minimum for all the $X_2H_5^+$ cations except $C_2H_5^+$. For $C_2H_5^+$, it collapses into the eclipsed classical form, but it corresponds to a neat shouldering on the potential energy surface. The four structures **1**–**4** mentioned above should therefore be the only possible isomers for the analogues of the ethyl cation.

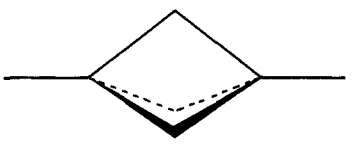

5

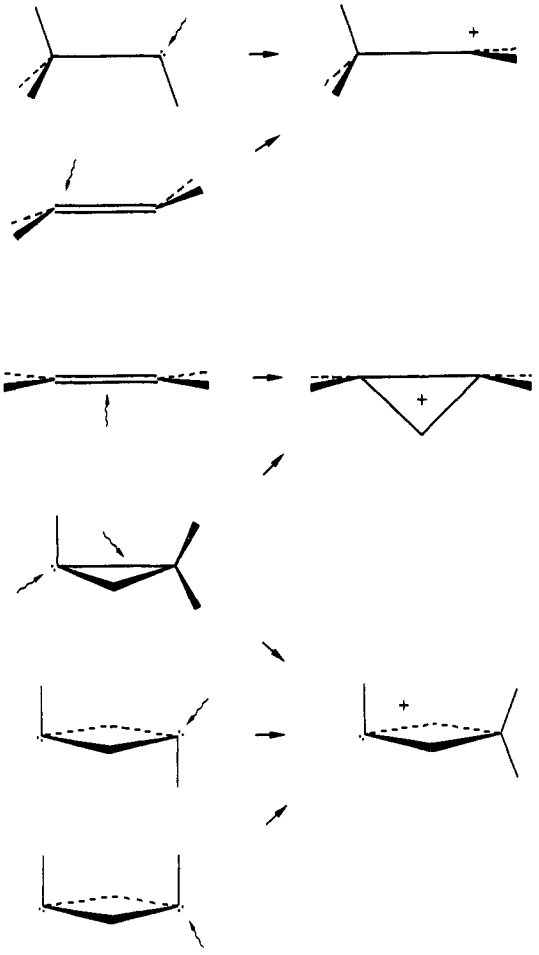

Figure 1. Different ways of protonating the various X_2H_4 isomers, with expected products.

At the SCF level, the classical form **1** is found to be a true minimum in all the surfaces and the nonclassical form **2** is found to be a true minimum for $C_2H_5^+$ and $Si_2H_5^+$. With the heavier atoms, structure **2** is a saddle point. Examination of the vibrational mode associated to the imaginary frequency indicates this is the transition state for hydrogen scrambling in the classical form, **6**. As mentioned, the doubly bridged structure **3** and the singly bridged structure **4** are true minima except for $C_2H_5^+$ where they only correspond to a shouldering on the potential surface. Since correlation effects may change the nature of the stationary points, some checks were made by performing CASSCF optimizations

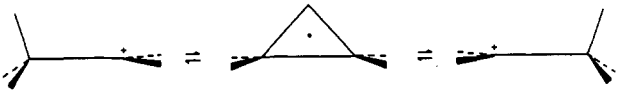

6

(5) Köhler, H.-J.; Lischka, H. *Chem. Phys. Lett.* **1983**, *98*, 454.
(6) Raghavachari, K. *J. Chem. Phys.* **1990**, *92*, 452.
(7) Curtiss, L. A.; Raghavachari, K.; Deutsch, P. W.; Pople, J. A. *J. Chem. Phys.* **1991**, *95*, 2433.
(8) Ruscic, B.; Berkowitz, J. *J. Chem. Phys.* **1991**, *95*, 2416.
(9) Trinquier, G. *Chem. Phys. Lett.* **1992**, *188*, 572.
(10) Raghavachari, K. *J. Chem. Phys.* **1991**, *95*, 7373.
(11) (a) Trinquier, G. *J. Am. Chem. Soc.* **1990**, *112*, 2130. (b) Trinquier, G. *J. Am. Chem. Soc.* **1991**, *113*, 144.
(12) Leszczynski, J.; Lammertsma, K. *J. Phys. Chem.* **1990**, *94*, 5543.
(13) Lammertsma, K.; Leszczynski, J. *J. Phys. Chem.* **1991**, *95*, 3941.

(14) Calculated geometrical parameters are as follows: Pb–Pb = 3.101 Å, $Pb-H_b$ = 2.067 Å, $Pb-H_t$ = 1.806 Å, PbH_bPb = 97.2°. At the SCF level, this structure lies 48 kcal/mol above the classical one.

with active spaces built on three-center two-electron sets corresponding to the X–H–X bridge in the nonclassical form, **7a**, and to its equivalent set (X–H + p_π) in the classical form, **7b**. With such treatment, we checked that (1) the classical form of $C_2H_5^+$ does collapse into the nonclassical C_{2v} structure **2**, (2) the true minimum character of the classical and nonclassical forms of $Si_2H_5^+$ remains unchanged, and (3) the saddle-point character for the nonclassical structure of $Pb_2H_5^+$ remains unchanged. The MCSCF procedure *decreases* (by 39 cm^{-1}) the *imaginary* frequency corresponding to the C_s mode that converts **2** into **1** in $Pb_2H_5^+$. In $Si_2H_5^+$, this mode is associated with a real frequency—the lowest one—which is now *increased* at the MCSCF level by a comparable amount of 36 cm^{-1}. From this constancy and from the values of the imaginary frequencies in the nonclassical forms **2** of $Ge_2H_5^+$ and $Sn_2H_5^+$ (see below), we can deduce that they should also keep their saddle-point character.

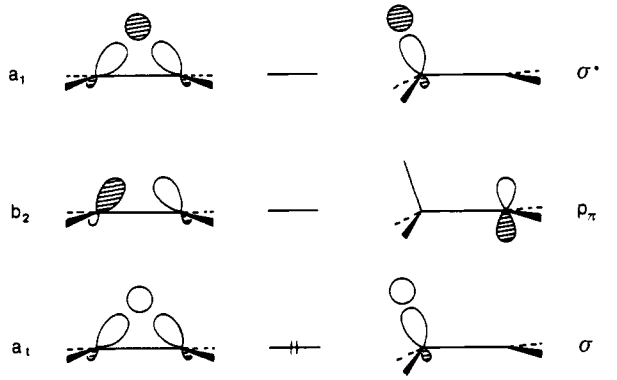

7

The features of the potential surfaces can finally be summarized by the index of the critical points associated with the three forms. With the best level of treatment they are estimated as follows (with 0 corresponding to a true minimum and 1 corresponding to a saddle point).

	1	**2**	**3**	**4**
C	1	0	–	–
Si	0	0	0	0
Ge	0	1	0	0
Sn	0	1	0	0
Pb	0	1	0	0

A further point that must be examined in a study involving several local minima is the position of the first vibrational level with respect to the energy barrier separating two minima on a given rearrangement coordinate. In practice, the position of the first vibrational level on the coordinate is given by the difference between the zero-point energy (ZPE) of the highest minimum and that of the transition state:

$$\Delta ZPE = \sum_{i=1}^{n} \frac{1}{2} h\nu_i - \sum_{i=1}^{n-1} \frac{1}{2} h\nu'_i$$

We will see below that the barriers separating **1** and **3** are high above the first vibrational levels along the corresponding coordinate. The barriers separating **3** and **4** are low but they are also located, at the SCF level, above the first vibrational level. In this rearrangement, solvation effects should enhance the barrier, so that **3** and **4** should be actually observable minima whenever a minimum does exist. The problem is less obvious for the **1–2** internal rearrangement in $Si_2H_5^+$. At the SCF level, the barrier for the **2** → **1** rearrangement is calculated at only 1.1 kcal/mol above **2**.[15] The first vibrational level of **2** along this coordinate lies at 0.7 kcal/mol[16] so that, here also, **2** is an observable minimum for $Si_2H_5^+$. In contrast, the calculated energy differences between the two conformations of the classical form, staggered **8** and eclipsed **9**, are too small to discriminate them at any temperature. Discarding the case of $C_2H_5^+$, the energies of these two conformations are nearly degenerate. The zero-point energy associated with the rotation around X–X in **8** is ≈0.1 kcal/mol (ν = 70–80 cm^{-1}, see Table II below), which is largely above the tiny energy differences between **8** and **9**. There is therefore a free rotation around X–X, and **8** and **9** constitute the same entity on the potential energy surface.

8 **9**

It may seem paradoxical that the singly bridged structures **2** do not exist for the heavier cations while a singly bridged structure was found to be a real minimum for neutral Sn_2H_4 and Pb_2H_4.[11] This can be accounted for through arguments that also explain why the singly bridged structure no longer exists when going from $Si_2H_5^+$ to $Ge_2H_5^+$. The doubly bonded form of disilene $H_2Si{=}SiH_2$ is found to be planar at an SCF level of calculation.[11] At a refined level which includes electron correlation, the molecule distorts into a trans-bent form, but the barrier to planarity remains quite small (≈1 kcal/mol). In contrast, digermene and the heavier analogues distort at the SCF level and have larger barriers to planarity. These results are consistent with the disappearance of the symmetrical C_{2v} doubly bridged SCF minimum when going from $Si_2H_5^+$ to $Ge_2H_5^+$. In other words, when the double bond bends, the $H_2X–XH_2$ part of the cyclic protonated form should do the same and open to give the classical isomer **10**. This is observed with germanium and with the heavier elements. It happens that the singly bridged isomer of neutral X_2H_4 only exists with tin and lead. Since these atoms give the strongest trans bending of the double bond, as soon as the cyclic cation is made by protonation of the extracyclic lone pair of the neutral isomer, it is spontaneously trapped in the deep minimum of the open classical form, **10**. Note that the X–X bond in the cyclic neutral molecule has heteropolar character so that the second X atom also has its lone pair available to some extent. The protonation of this lone pair rather than the extracyclic one leads to the doubly bridged form of the cation, as indicated in Figure 1.

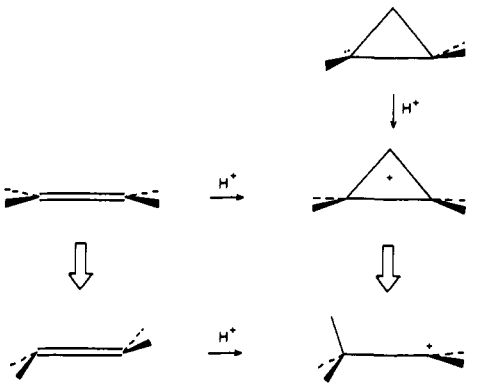

10

Structures

The SCF-calculated geometrical parameters for the various isomers and for the dissociation fragments are all listed in Table

(15) At the MP4 level, the barrier is significantly larger, see below.

(16) This value is obtained from ΔZPE. Another estimate is given from the lowest vibrational frequency in **2**. This frequency is assigned to a mode that clearly anticipates the **2** → **1** rearrangement. The energy $^1/_2h\nu$ associated with this frequency is calculated at 0.5 kcal/mol.

Table I. SCF-Calculated Geometries[a]

		C		Si		Ge	Sn	Pb	
				Fragments					
HX_3^+	X-H	1.089		1.452		1.522	1.686	1.711	
XH_4	X-H	1.092		1.473		1.547	1.710	1.740	
XH^+ ($^1\Sigma^+$)	X-H	1.117		1.488		1.578	1.750	1.807	
XH_2 ($^1A_1$)	X-H	1.106		1.508		1.597	1.768	1.832	
	HXH	102.5		93.7		93.0	92.5	92.0	
				Classical (C_s) **1**					
X_1-X_2		1.418	1.438[b]	2.388	2.389[b]	2.566	2.882	2.981	2.981[b]
X_1-H_1		1.136	1.086	1.465	1.461	1.534	1.695	1.718	1.716
X_1-H_2		1.088	1.104	1.461	1.464	1.531	1.693	1.716	1.718
X_2-H_3		1.089	1.089	1.462	1.462	1.537	1.702	1.745	1.745
$X_1X_2H_3$		121.3	123.1[c]	123.7	124.6[c]	124.3	125.0	126.4	127.0[c]
$X_2X_1H_1$		90.2	115.0	102.1	104.9	101.5	101.2	99.0	100.7
$X_2X_1H_2$		116.5	106.8	104.3	102.9	103.4	102.6	100.3	99.7
$H_2X_1H_2$		116.1	102.8	115.2	114.2	115.7	116.0	117.5	117.3
$H_1X_1H_2$		106.5	112.2	114.4	114.9	115.0	115.6	116.9	116.8
$H_3X_2H_3$		117.0	116.5	112.7	112.6	111.3	109.9	107.2	107.2
				Nonclassical (C_{2v}) **2**					
X-X		1.375	1.379[d]	2.180	2.182[d]	2.329	2.629	2.696	2.694[d]
X-H_b		1.317	1.333	1.696	1.712	1.815	1.976	2.072	2.103
X-H_t		1.086	1.085	1.455	1.455	1.524	1.685	1.712	1.713
φ[e]		−1.3	−1.8	8.9	8.4	10.1	12.3	13.2	12.4
H_bXX		58.5	58.9	50.0	50.4	50.1	50.5	49.4	50.2
XH_bX		62.9	62.2	80.0	79.2	79.8	79.0	81.2	79.7
H_tXH_t		118.6	118.5	121.2	121.2	121.1	120.9	122.1	121.9
				Doubly Bridged (C_s) **3**					
X_1-X_2		1.638[f]		2.602		2.861	3.105	3.289	
X_1-H_b		1.345		1.860		2.088	2.183	2.384	
X_2-H_b		1.197		1.532		1.610	1.782	1.818	
X_1-H_1		1.092		1.491		1.579	1.753	1.812	
X_2-H_2		1.089		1.453		1.523	1.683	1.707	
X_2-H_3		1.094		1.454		1.524	1.685	1.709	
θ[g]		28.5		3.6		2.7	7.6	7.0	
$X_1H_bX_2$		79.6		99.8		100.6	102.6	102.2	
$H_bX_1H_b$		89.3		70.9		67.1	67.8	65.2	
$H_bX_2H_b$		105.4		89.5		91.6	86.3	89.9	
$H_1X_1X_2$		99.8		81.9		81.2	77.2	78.2	
$X_1X_2H_2$		121.7		119.7		119.3	116.8	115.8	
$X_2X_2H_3$		120.8		119.3		120.0	121.9	122.3	
$H_2X_2H_3$		117.5		121.0		120.6	121.3	121.9	
$H_2X_2H_b$		116.8		112.0		111.0	112.3	110.8	
$H_3X_2H_b$		98.7		108.9		109.4	109.7	109.4	
				Singly Bridged (C_s) **4**					
X_1-H_b		1.287[f]		1.600		1.683	1.837	1.901	
X_2-H_b		1.269		1.747		1.851	1.990	2.097	
X_1-H_1		1.084		1.457		1.528	1.691	1.716	
X_1-H_2		1.084		1.458		1.529	1.692	1.718	
X_2-H_3		1.108		1.491		1.581	1.754	1.816	
$X_1H_bX_2$		173.0		174.8		163.4	157.0	153.1	
$H_bX_2H_3$		98.8		85.8		86.7	85.3	85.9	
$H_1X_1H_b$		96.4		101.1		100.4	100.3	99.6	
$H_2X_1H_b$		102.0		101.5		101.7	101.3	101.0	
$H_2X_1H_2$		117.1		116.1		116.0	116.2	116.9	

[a] In Å and deg. See Figure 2 for atom labeling. [b] This column refers to the eclipsed conformation. [c] For the XH_2-eclipsing bond. [d] This column refers to MCSCF optimization from an active space localized on the X-H_b-X frame. [e] Tilt angle defined as the supplement of (H_tXH_t, XX); positive value corresponds to tilting towards H_b. [f] This column, for carbon, refers to a simple shouldering on the potential surface. [g] Puckering of the four-membered ring, defined as the supplement of ($H_bX_1H_b$, $H_bX_2H_b$); positive value corresponds to puckering toward H_1 and H_2.

I. The atom definitions for **1**, **2**, **3**, and **4** are given in Figure 2. The corresponding harmonic vibrational frequencies are listed in Table II.

Let us comment on the geometries of the classical forms **1**. For the staggered conformations, the case of carbon is different from the other elements since it prefigures the C_{2v} singly bridged form which it collapses into at higher level of description. Putting aside this atypical structure, let us try to figure out trends in the geometries of the other classical forms H_3X-XH_2^+. First, there are only minor differences in the corresponding geometrical parameters between the staggered and eclipsed conformations, which are nearly degenerate in energy. Such virtually equivalent atomic arrangements can be viewed from two different ways: (1) First, one usually considers **1** as a methyl-like cation XH_3^+ in which one hydrogen atom is substituted by a methyl-like group XH_3. In such a view, the two substructures embodied in the classical isomer are a methane-like arrangement and a methyl cation-like arrangement, **11**. (2) At the other extreme, and given what we

11

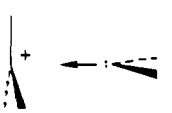

12

know about the relative stabilization of divalent forms with heavier

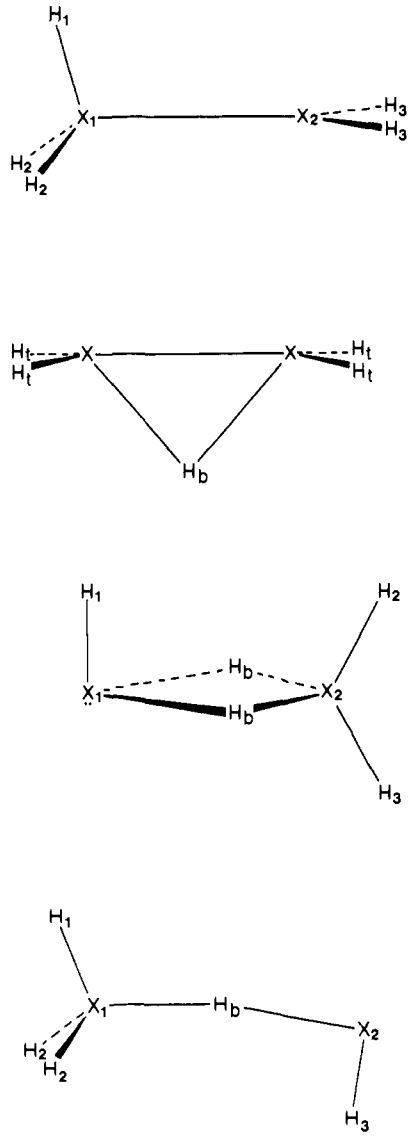

Figure 2. Atom labeling for the geometry descriptions.

elements, the classical form **1** can also be viewed as a complex between a singlet carbene and a methyl cation, **12**. Examination of the distances and angles suggest that **11** is the best mental geometry decomposition in all cases, although the proximity to **12** is more and more discernible when going down to heavier elements. This trend is also supported by the net atomic charges, listed in Table III.

The calculated geometries for nonclassical singly bridged $C_2H_5^+$ and $Si_2H_5^+$ are in agreement with those previously published in the literature.[5-7] Note that the optimizations performed at the MCSCF level, with an active space localized on the $X-H_b-X$ frame, are quite close to those optimized at the SCF level. As noticed previously,[5] the tilting of the extracyclic XH_2 group occurs outside the bridging hydrogen in $C_2H_5^+$, whereas it occurs toward it in $Si_2H_5^+$ and its heavier analogues. This tilt angle regularly increases form Si to Pb. A similar trend was observed from singly bridged Sn_2H_4 to singly bridged Pb_2H_4 although in these neutral local minima such tilt angles were significantly larger than in the present cationic saddle points (20° and 35°, respectively).[11b] The three-membered ring is more prolate in $C_2H_5^+$ than in the heavier analogues where it has a similar shape for all, quite close to a right-angle triangle.

It is interesting to determine where the positive charge is located in C_{2v} nonclassical $X_2H_5^+$. One can see in Table III that the positive charge is shared by all the hydrogen atoms in $C_2H_5^+$, whereas it is mainly located on the X atoms in $Si_2H_5^+$ and in the following analogues.

Table II. SCF-Calculated Harmonic Vibrational Frequencies (cm^{-1})

	C	Si	Ge	Sn	Pb
		Classical (C_s) **1**			
1a″	551	83	76	69	78
1a′	293	411	224	162	105
2a″	893	408	360	301	256
2a′	1219	457	420	360	351
3a″	1305	665	585	479	454
3a′	1334	740	650	536	508
4a′	1439	932	827	708	663
4a″	1413	1007	931	793	757
5a′	1565	1015	936	796	758
6a′	1657	1062	973	839	809
7a′	2849	2395	2238	2103	1939
5a″	3351	2427	2250	2110	1954
8a′	3252	2405	2267	2137	2023
6a″	3397	2439	2270	2139	2032
9a′	3278	2425	2271	2147	2038
		Nonclassical (C_{2v}) **2**			
$1b_1$	425	327	200i	136i	414i
$1a_1$	1223	597	343	242	168
$1b_2$	902	421	380	316	302
$1a_2$	1136	581	541	446	434
$2a_2$	1336	655	580	471	455
$2a_1$	1428	762	703	604	599
$2b_1$	1384	948	858	720	652
$2b_2$	1233	982	887	790	735
$3a_1$	1696	1010	929	793	766
$3b_1$	1568	1185	1004	988	832
$4a_1$	2316	1692	1529	1451	1332
$4b_1$	3283	2428	2284	2145	2018
$5a_1$	3290	2430	2285	2146	2017
$3a_2$	3397	2471	2301	2158	2043
$3b_2$	3413	2478	2308	2165	2052
		Doubly Bridged (C_s) **3**			
1a′		289	169	139	95
2a′		329	245	238	217
1a″		485	241	343	219
2a″		663	553	503	435
3a′		785	671	557	499
4a′		993	885	758	712
3a″		998	913	800	765
5a′		1041	922	847	779
4a″		1199	1002	936	848
6a′		1336	1112	1059	940
5a″		1964	1832	1711	1587
7a′		2106	1971	1858	1722
8a′		2273	2088	1969	1773
9a′		2447	2304	2169	2058
10a′		2493	2318	2187	2072
		Single Bridged (C_s) **4**			
1a′		225	79	60	43
1a″		256	84	100	95
2a″		297	180	169	166
2a′		304	256	263	257
3a′		732	645	547	505
4a′		921	812	716	672
3a″		1000	864	774	726
5a′		1020	929	791	757
4a″		1021	932	792	759
6a′		1088	973	924	863
7a′		1921	1770	1781	1575
8a′		2298	2099	1968	1789
9a′		2416	2279	2148	2027
5a″		2453	2282	2147	2027
10a′		2453	2283	2150	2031

The doubly bridged structures have a nearly planar four-membered ring, only slightly puckered and significantly distorted from the regular rhombuses of doubly bridged X_2H_4, as illustrated in **13** for Si and Pb. Comparison of these doubly bridged geometries with the geometries of the fragments XH^+ and XH_4 (see Table I) clearly suggests that these structures can be viewed as the adduct (HX^+, XH_4). Not only are the X_1-H_b bonds longer

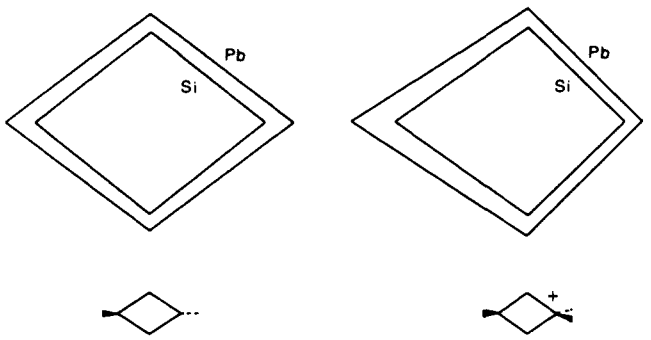

13

than those of X_2–H_b, but the X_1–H_1 bond lengths are remarkably close to those in XH^+, while the X_2–H_2 and X_2–H_3 lengths are not far from those in XH_4 (about 0.03 Å shorter). If the X_2H_b bond is longer than that in XH_4, the $H_bX_2H_2$ and $H_bX_2H_3$ angles are not far from the tetrahedral angle. This picture is supported to some extent by the atomic populations listed in Table III. Discarding the case of carbon, the X_1H_1 set carries most of the positive charge, even though all atomic charges are perturbed with respect to those in the isolated fragments. Remarkably, the doubly bridged geometry of $C_2H_5^+$ exhibits the same trends although it only corresponds to a shouldering on the potential surface. This suggests that such an atomic arrangement actually remains a potential binding scheme, even when it is not materialized as a true minimum on the potential energy surface.

It is interesting to see what occurs to the formal positive charge when a doubly bridged neutral molecule X_2H_4 is protonated. As soon as the proton approaches one of the two extracyclic lone pairs, the X center is in a tetrahedral environment (the mechanism is equivalent for the cis and trans isomers). To recover a methane-like XH_4 bonding scheme, the X center tends to pull the electron pairs of the symmetrical bridges toward itself in order to make the H_b–X bonds close to regular two-center two-electron bonds. This breaks the symmetry of the bridges and entails a migration of the positive charge toward the opposite XH fragment, which formally becomes XH^+, **14**. A simple way to understand why the doubly bridged arrangement produces such a partition

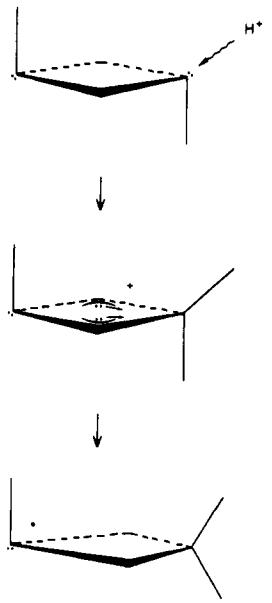

14

is to remember that it is much easier to ionize an :Ẋ–H species of group 14 (in its $^2\Pi$ ground state) than a methane-like XH_4 species. In the latter system, all occupied energy levels are deep since they all correspond to σ bonds, while in the former system there are three nonbonding electrons located in high-lying levels.

The doubly bridged form of the $X_2H_5^+$ cation can therefore be viewed as a complex between an XH^+ fragment and an XH_4 molecule. The complex is bound through two three-center two-electron bridges built from two X–H bonds of XH_4 and the two empty p orbitals of XH^+ in its $^1\Sigma^+$ ground state, the lone pair on XH^+ remaining basically unchanged, **15**. Because of this delocalization, XH^+ abandons part of its charge to the benefit of XH_4,

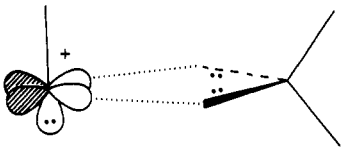

15

explaining the atomic charges of Table III. To the extent that this sharing is not total and the dissymmetry of the bridges is preserved, this isomer is still better described as the adduct $XH^+ + XH_4$.

The structure of the singly bridged form **4** has been described by Raghavachari in the case of $Si_2H_5^+$.[10] It is also, clearly, the H_3X–H···XH^+ ion-molecule complex. Discarding the case of $C_2H_5^+$, its features are common in the whole series. The two X–H_b distances are different, here, from those in the doubly bridged system. In both cases, the "intermolecular" X–H_b bond is longer than the "intramolecular" one, but the effect is more marked in **3** than in **4**, as can be seen in Table I. A similar trend has been observed in the singly and doubly bridged forms of $Si_2H_4^+$.[17] The net atomic charges (Table III) favor the H_3X–H + XH^+ partition over H_3X^+ + H–XH. Since H_b bears a large negative charge, Table III rather suggests $H_3X^+ + H^- + XH^+$ as the best partition. Complex **4** therefore owes much of its stability to this linear arrangement X^+–H^-–X^+ of the partial charges. In this sense, the bonding in **4** is mainly due to polarization effects, whereas there are more delocalization components in **3**. Remarkably, the two bridges in **3** have about the same bond strength as the single bridge in **4** since both systems happen to have a similar binding energy with respect to $XH_4 + XH^+$ (see below). From the point of views of both the geometry and the charges, the H_2C–H–CH^+ shouldering is closer to the H_3C^+ + H–CH complex than to the H_3C–H + CH^+ one, in agreement with the relative stability of the two sets of fragments. The case of carbon is the only one where the $CH_3^+ + CH_2$ set is favored, at least at the SCF level, over $CH_4 + CH^+$.

It is interesting to compare the X–X bond lengths in the first three forms of the cations with typical X–X single bond lengths, as they are calculated under similar conditions in the D_{3d} ethane-like molecules H_3X–XH_3. Such a comparison is made in Figure 3. Except for carbon, the regular single bond lengths stand just in between those in **1** and **2**. Protonation of a doubly bonded form therefore does not restore a single bond length. For planar ethylene and disilene, it only lengthens the XX bond by about 0.05 Å, while for trans-bent digermene and distannene it modifies it by +0.01 and −0.08 Å, respectively. One may consider, in effect, that the protonation of the trans-bent double bond into the symmetrical singly bridged cation **2** changes the nature of the double dative bond into a more covalent one. The XX bond lengths in the classical forms keep nearly unchanged with respect to those in the nonprotonated methylmethylene-like forms H_3X–XH.[11] In the doubly bridged cations **3**, the XX distances are even longer than those in the nonprotonated doubly bridged molecules (by 0.02–0.06 Å), so they can hardly be considered to fall within the zone of linked atoms. Note in Figure 3 that, except for carbon, the XX lengthening occurring from **2** to **1** is about the same as that occurring from **1** to **3**. Again, the case of carbon is singular in this figure. The classical form (in its staggered or eclipsed conformation) happens to have a C–C bond shorter than that calculated for ethane and close to that calculated for the singly bridged form. This originates in the hyperconjugation taking place between the p_π empty orbital on C_2 and the σ occupied orbital

(17) Raghavachari, K. *J. Chem. Phys.* **1988**, *88*, 1688.

Table III. Net Atomic Charges (Mulliken Definition)

		C	Si	Ge	Sn	Pb
XH^+ ($^1\Sigma^+$)	X	+0.76	+1.06	+0.99	+1.08	+1.07
	H	+0.24	−0.06	+0.01	−0.08	−0.07
XH_2 ($^1A_1$)	X	−0.07	+0.41	+0.31	+0.45	+0.42
	H	+0.03	−0.20	−0.16	−0.23	−0.21
XH_3^+	X	+0.33	+1.02	+0.82	+1.00	+0.85
	H	+0.22	−0.01	+0.06	+0.00	+0.05
XH_4	X	−0.10	+0.76	+0.54	+0.78	+0.58
	H	+0.03	−0.19	−0.14	−0.19	−0.15
classical (C_s) **1**	X_1	−0.13[a]	+0.56	+0.46	+0.69	+0.57
	X_2	+0.24	+0.68	+0.56	+0.69	+0.58
	H_1	+0.15	−0.07	−0.02	−0.09	−0.02
	H_2	+0.17	−0.07	−0.02	−0.09	−0.02
	H_3	+0.20	−0.02	+0.02	−0.06	−0.04
	$X_1 + H_1 + 2H_2$	+0.36	+0.35	+0.50	+0.43	+0.50
	$X_2 + 2H_3$	+0.64	+0.65	+0.50	+0.57	+0.50
nonclassical (C_{2v}) **2**	X	+0.06	+0.59	+0.48	+0.68	+0.57
	H_b	+0.14	−0.19	−0.11	−0.20	−0.18
	H_t	+0.19	+0.00	+0.04	−0.04	+0.01
doubly bridged (C_s) **3**	X_1	+0.04[b]	+0.68	+0.66	+0.78	+0.82
	X_2	−0.02	+0.80	+0.60	+0.88	+0.71
	H_b	+0.19	−0.18	−0.12	−0.21	−0.20
	H_1	+0.16	−0.08	−0.04	−0.13	−0.11
	H_2	+0.21	−0.02	+0.02	−0.05	−0.01
	H_3	+0.20	−0.02	+0.02	−0.05	−0.01
	$X_1 + H_1$	+0.22	+0.60	+0.62	+0.65	+0.71
	$X_2 + 2H_b + H_2 + H_3$	+0.78	+0.40	+0.38	+0.35	+0.29
singly bridged (C_s) **4**	X_1	+0.12[b]	+0.92	+0.66	+0.90	+0.73
	X_2	+0.38	+0.91	+0.79	+0.91	+0.90
	H_b	−0.17	−0.53	−0.35	−0.40	−0.39
	H_1	+0.18	−0.06	−0.01	−0.08	−0.03
	H_2	+0.17	−0.07	−0.02	−0.09	−0.04
	H_3	+0.16	−0.10	−0.05	−0.14	−0.13
	$X_1 + H_1 + 2H_2 + H_b$	+0.47	+0.19	+0.26	+0.23	+0.23
	$X_2 + H_3$	+0.54	+0.81	+0.74	+0.77	+0.77
	$X_1 + H_1 + 2H_2$	+0.64	+0.72	+0.61	+0.64	+0.61
	$X_2 + H_b + H_3$	+0.37	+0.28	+0.39	+0.36	+0.39
dipole moments[c]	1	1.75	2.47	2.07	1.73	0.27
	2	0.79	0.56	0.48	0.90	1.13
	3	2.63	0.89	0.45	0.11	1.31
	4	1.82	1.47	1.53	1.76	2.29

[a] For carbon, this column refers to the eclipsed conformation. [b] For carbon, this structure corresponds to the shouldering on the potential surface. [c] In Debyes.

Table IV. Relative Energies[a]

		SCF					MP4				
		C	Si	Ge	Sn	Pb	C	Si	Ge	Sn	Pb
	$X_2H_4 + H^+$	176.1	217.5	219.5	207.5	194.2	172.3	208.7	207.3	204.9	190.8
	$XH_3^+ + XH_2$	126.7	61.3	51.7	47.0	45.7	150.7	65.4	55.3	55.5	50.6
	$XH^+ + XH_4$	138.4	41.1	30.7	21.9	20.6	151.3	41.4	32.3	29.7	26.1
$X_2H_5^+$	doubly bridged C_s **3**	109.4[b]	21.5	12.7	0.2	1.3	102.9	12.0	5.5	0	0
	singly bridged C_s **4**	117.4[b]	20.7	11.1	0	0	117.2	16.6	7.8	3.7	1.5
	classical C_s **1**	0.4	0	0	1.0	13.1	7.6[d]	0.1	0	7.3	15.6
	nonclassical C_{2v} **2**	0	6.3	11.5[c]	12.9[c]	30.8[c]	0	0	5.3	13.2	26.5

[a] In kcal/mol. The fragments correspond to the preferred isomer for X_2H_4 (see ref 10), the $^1A_1$ state for XH_2 and the $^1\Sigma^+$ state for XH^+. [b] Not a critical point. [c] Saddle point. [d] Eclipsed conformation.

localized on the C_1H bonds of the CH_3 group. The resulting short C–C bond certainly favors the catching of this structure by the nonclassical minimum on the potential surface. The absence of strong hyperconjugation effects would explain why this no longer occurs with the silicon atom.

Energetics

The relative energies for all forms of $X_2H_5^+$ and their dissociation products are listed in Table IV, at both SCF and MP4 levels.[18] As mentioned, and in agreement with previous studies,[6,7] electronic correlation brings the classical and nonclassical forms of $Si_2H_5^+$ at about the same energy. On all the surfaces, only, the **3** and **4** ordering is changed by the correlation effects, both forms remaining close in energy. In the following, we restrict the discussion to the MP4 relative energies.

For $Si_2H_5^+$, the present results are in agreement with previous ones.[6,10] The classical and nonclassical forms are nearly degenerate in energy, with the singly bridged form **4** lying 17 kcal/mol above. The new result, here, is the presence of the doubly bridged isomer **3**, lying about 5 kcal/mol below the singly bridged form. In all the series, **3** is always favored over **4** by 1.5–4.6 kcal/mol. For germanium, the classical form is still preferred, whereas for tin and lead, the bridged forms are preferred. The doubly bridged form is therefore the absolute minimum for $Sn_2H_5^+$ and $Pb_2H_5^+$,

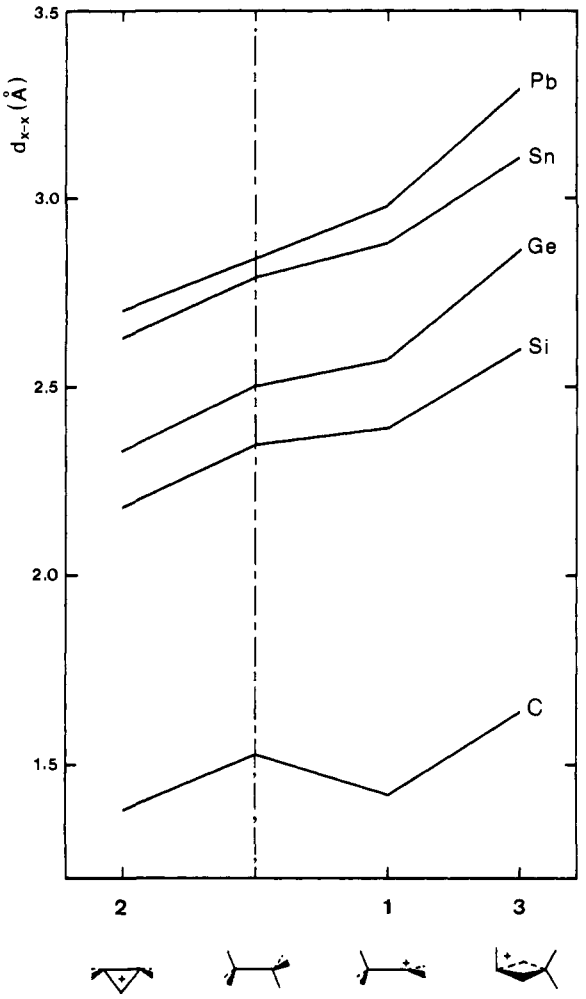

Figure 3. Comparison of the SCF-calculated X–X bond distances in the $X_2H_5^+$ cations and in typically single-bonded staggered H_3X–XH_3.

with the classical forms lying 7 and 16 kcal/mol above, respectively.

Since the two bridged forms are rather close in energy, they also have close binding energies with respect to fragments XH_4 and XH^+. This means the single bridge in **4** exhibits as much bonding as the two bridges in **3**. As mentioned, the single bridge is mainly bound through electrostatic interaction arising from the alignment of highly charged bridge atoms X^+–H^-–X^+. This happens to be almost twice as strong as the sum of polarization and delocalization occurring in each bridge of the four-membered doubly bridged ring system.

Most barriers separating the various minima were calculated by determining the corresponding saddle points at the SCF level. First, the transition state for the interconversion of the classical form of $Si_2H_5^+$ into its nonclassical form corresponds to an energy barrier which is calculated at only 1.1 kcal/mol (SCF level) above the C_{2v} nonclassical form.[19] This value is weak since such internal rearrangement is allowed (see **7**) and since the classical form lies 6 kcal/mol below the nonclassical form at this level of theory. At the MP4 level, both isomers are nearly degenerate in energy, and the barrier is raised as expected from Hammond postulate arguments; it is calculated at 2.8 kcal/mol.

Table V. Energy Barriers on the C_s Pathway Relating the Classical Form **1** and the Doubly Bridged Form **3**[a]

	SCF			MP4		
	1	TS	**3**	**1**	TS	**3**
Si	0	50.7	21.5	0	33.1	12.0
Ge	0	46.1	12.7	0	29.2	5.5
Sn	1.0	40.2	0	7.3	30.2	0
Pb	13.1	46.0	0	15.6	33.7	0

[a] In kcal/mol. TS stands for transition state. For Ge and Sn, its energy is estimated by interpolation from the results for Si and Pb (see text).

Table VI. How Structural Trends Can Be Obtained from Simple Ratios[a]

problem	relevant ratio[a]	1/2	1
double bond	$\frac{\sum\Delta E_{ST}}{E_{\sigma+\pi}}$	planar trans-bent	no direct double link
single bond versus bridge	$\frac{n\text{BBB}}{E_\sigma}$	$(H-)_n$–X–X preferred	:X–$(-H-)_n$–X preferred

[a] $E_{\sigma+\pi}$ and E_σ correspond to the XX bond energies. $\sum\Delta E_{ST}$ is the sum of the singlet–triplet separations for the two fragments of the double bond. BBB (bridge bonding benefit) is the binding energy of an electron-deficient bridge X–H–X with respect to X–H + X.

Let us now consider the pathway connecting the classical form **1** to the doubly bridged form **3**. A least-motion path may start from the eclipsed conformation of the classical form and will reach the doubly bridged form through a simple rocking of the two X_1–H_2 bonds, **16**, the C_s symmetry being preserved during the transit. Let us examine whether or not this rearrangement is symmetry-allowed. Discarding the three X–H bonds which are not changed during the reaction, the relevant orbitals are as

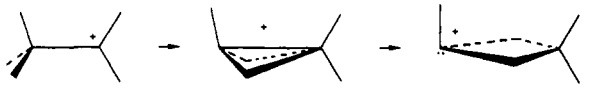

16

follows. In the starting material, we have three occupied σ orbitals. Two of them are the symmetrical and antisymmetrical combinations of the σ_1 and σ_2 orbitals corresponding to the X_1–H_2 bonds, and the third one corresponds to the X_1–X_2 bond. Each of these σ orbitals has its antibonding σ^* counterpart. Last, we have an empty p_π orbital on X_2, which is antisymmetrical with respect to the mirror plane, **17**. The corresponding seven orbitals of the final product are the classical set of the electron-deficient double bridge (six orbitals, two of them occupied, labeled as in diborane for convenience) plus an occupied n_σ orbital corresponding to the lone pair on X_1, **18**. When all these orbitals are assigned their symmetrical or antisymmetrical character with respect to the relevant symmetry plane, the reaction appears to be—at least formally—symmetry-allowed. We therefore expect a low barrier for such a path. The transition states were determined for $Si_2H_5^+$ and $Pb_2H_5^+$.[20] For $Pb_2H_5^+$, it corresponds to a real saddle point with one imaginary frequency at 971 cm^{-1} corresponding to the mode depicted in **19**. For $Si_2H_5^+$, the real transition state is slightly distorted from the C_s symmetry.[21] At the SCF level, these

(18) The zero-point vibrational energies are not taken into account in this table. They are quite close from one isomer to another and would only decrease the dissociation enthalpies by about 3 kcal/mol at the SCF level.

(19) This value is in agreement with that reported by Raghavachari in ref 6. Our SCF-optimized transition state (Si_1–Si_2 = 2.231 Å, Si_1–H_1 = 1.545 Å, Si_2–H_1 = 2.078 Å, Si_1–H_2 = 1.455 Å, Si_2–H_3 = 1.459 Å) however differs from his in the $Si_1H_1Si_2$ ring geometry. Calculated with our pseudopotentials and our basis sets, that geometry is found to lie only 0.05 kcal/mol below ours. The potential surface is therefore very flat along this coordinate.

(20) Using the labeling of Figure 2, the SCF-calculated geometrical parameters for these stationary points are as follows (in Å and deg). $Si_2H_5^+$: Si–Si = 2.347, Si_1–H_b = 1.511, Si_2–H_b = 1.892, Si_1–H_1 = 1.467, Si_2–H_2 = 1.465, Si_2–H_3 = 1.460, SiH_bSi = 82.3, $H_bSi_1H_b$ = 99.1 $H_bSi_2H_b$ = 69.9, $Si_2Si_1H_1$ = 87.0, $Si_1Si_2H_2$ = 128.9, $Si_1Si_2H_3$ = 117.3. $Pb_2H_5^+$: Pb–Pb = 3.022, Pb_1–H_b = 1.795, Pb_2–H_b = 2.013, Pb_1–H_1 = 1.752, Pb_2–H_b = 1.750, Pb_2–H_3 = 1.746, PbH_bPb = 85.7, $H_bPb_1H_b$ = 98.7, $H_bPb_2H_b$ = 64.0, $Pb_2Pb_1H_1$ = 84.0, $Pb_1Pb_2H_2$ = 127.7, $Pb_1Pb_2H_3$ = 122.0. The two structures exhibit a good isomorphism.

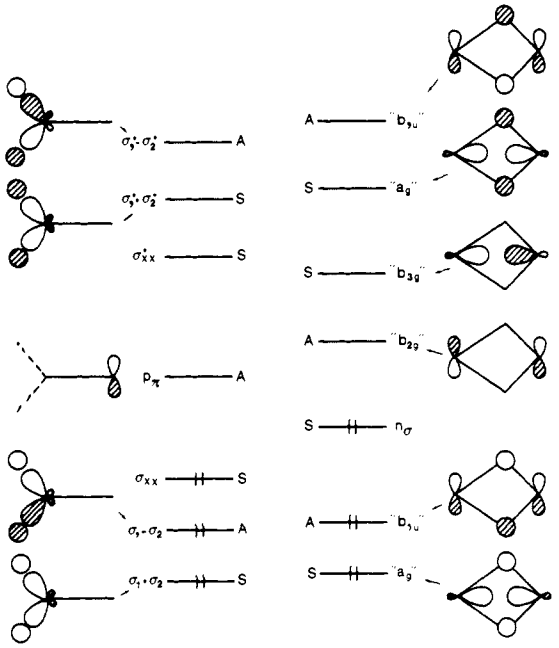

17 18

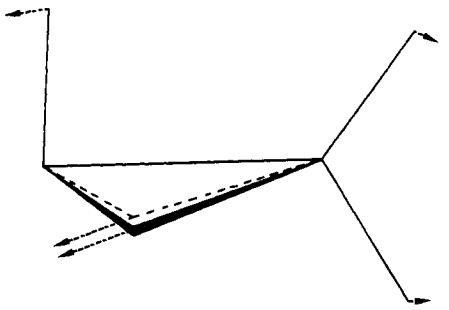

19

transition states are located at 50 (Si) and 33 kcal/mol (Pb) above the classical form. At the MP4 level, these barriers reduce to 31 and 18 kcal/mol, respectively. Noticing that the heights of the C_s barriers with respect to the averaging energy between starting and final products are rather constant (SCF, 40.0 and 39.5 kcal/mol; MP4, 27.1 and 25.9 kcal/mol), we used them to estimate the barriers for germanium and tin. The full set of C_s barriers is given in Table V. For an allowed process, these barriers are unexpectedly high. A close look at the correlation diagram relating **18** to **17** is necessary. Extended Hückel calculations were performed for a linear synchronous transit corresponding to the rearrangement **16** in both $Si_2H_5^+$ and $Pb_2H_5^+$. Examination of the resulting Walsh diagrams indicates that there are avoided level crossings between occupied and virtual a′ levels. The diagrams are rather complex because of the mixings in the a′ symmetry, but careful analysis suggests that the σ_{xx} orbital in **17** in fact correlates with the virtual "ag" orbital in **18**, while the σ^*_{xx} level in **17** in fact correlates with the n_σ level in **18**. Obviously, the reaction is formally symmetry-allowed by physically (or intrinsically) forbidden, which accounts for the large barriers. In the most favorable cases, **1** → **3** for Pb and **3** → **1** for Si, these barriers are estimated at 18 and 19 kcal/mol, respectively.

The other ways the doubly bridged structures can evolve is (1) the natural dissociation into $XH^+(^1\Sigma^+)$ and XH_4, a process which requires no supplementary barrier (as we checked for $Si_2H_5^+$) but which is endothermic by as much as 27–30 kcal/mol (see below), and (2) the ring opening into the singly bridged form. The saddle points relating the two forms **3** and **4** of the ion–molecule complexes were determined for $Si_2H_5^+$ and $Pb_2H_5^+$. A natural pathway to go from **4** to **3** will begin by simple rotations around X_1–H_b and X_2–H_b, followed by a H_1–X_2 closure, **20**. Such a pathway may seem rather complex, but it only involves the formation of a "partial" bond. In a similar problem on $Si_2H_4^+$, Raghavachari predicted that the corresponding barrier is expected to be low.[17] Indeed, our calculated barriers are very low. At the SCF level, the **3** → **4** exothermic conversions require barriers of 2.1 kcal/mol for $Si_2H_5^+$ and 0.5 kcal/mol for $Pb_2H_5^+$. At the MP4 level, the **4** → **3** rearrangements are now exothermic, and the corresponding barriers reduce to 0.5 and 0.2 kcal/mol, respectively. The two intermolecular forms **3** and **4** are therefore easily convertible into each other, although their bridge bonds are somewhat different in nature.

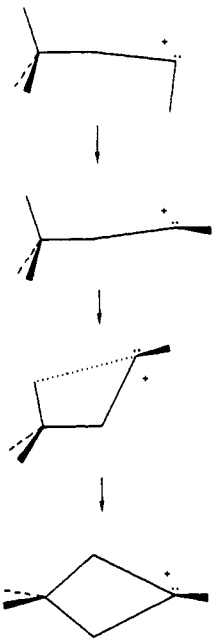

20

The barrier between the classical form **1** and the singly bridged form **4** has been calculated by Raghavachari for $Si_2H_5^+$: at the MP4 level this transition state is located 22 kcal/mol above **4**.[17] This is not far from the MP4 barrier calculated for the **3** → **1** interconversion (19 kcal/mol). The clustering reaction of SiH^+ with silane giving **1** could therefore proceed via intermediates **3** or **4** with about equal activation energies.

With these energy barriers, we can now represent the shape of the whole potential surfaces. As in previous works,[11,22] we

(21) For $Si_2H_5^+$, the imaginary frequency corresponding to **19** occurs at 1231 cm^{-1}, but there is in this case an additional imaginary frequency, at 334 cm^{-1}, associated with an a″ dissymetrical deformation. When distorted according to this mode, the system relaxes into the classical form, through a pathway which first winds in the vicinity of the nonclassical arrangement. The saddle-point research in the a″ distortion deformation leads to a C_1 saddle point, only slightly deformed with respect to the C_s one, and lying at 0.9 kcal/mol (SCF) and 2.6 kcal/mol (MP4) below it (with geometrical parameters as follows, in Å and deg: Si–Si = 2.349, Si_1–H_b = 1.485 and 1.561, Si_2–H_b = 2.245 and 1.767, Si_1–H_1 = 1.472, Si_2–H_2 = 1.461, Si_2–H_3 = 1.459, SiH_bSi = 75.0 and 89.5, $H_bSi_1H_b$ = 97.8, $H_bSi_2H_b$ = 68.7, $Si_2Si_1H_1$ = 79.7, $Si_1Si_2H_2$ = 124.0, $Si_1Si_2H_3$ = 120.2, dihedral $H_1Si_1Si_2H_2$ = 27.1, $H_1Si_1Si_2H_3$ = −163.3). This unsymmetrical saddle point might also correspond to that separating the C_{2v} nonclassical minimum **2** from the C_s doubly bridged minimum **3**. However, geometry relaxation in the direction of the imaginary frequency (at 1047 cm^{-1}) leads to the classical form. The case of $Si_2H_5^+$ is complicated because the two saddle points for the **1** → **3** and **2** → **3** internal rearrangements can be in the same region of the potential hypersurface. Moreover, the two forms of **1**, eclipsed and staggered, are nearly degenerate in energy, which could make this region rather flat and explain the observed distortion. Anyway, the problem would deserve to be further investigated at higher level of calculation (MP4 or MCSCF). Since **2** is no longer a minimum in the heavier compounds, they all should behave as $Pb_2H_5^+$. Note that in the C_s transition state of $Pb_2H_5^+$ the above-mentioned a″ deformation mode corresponds to a low real frequency (80 cm^{-1}).

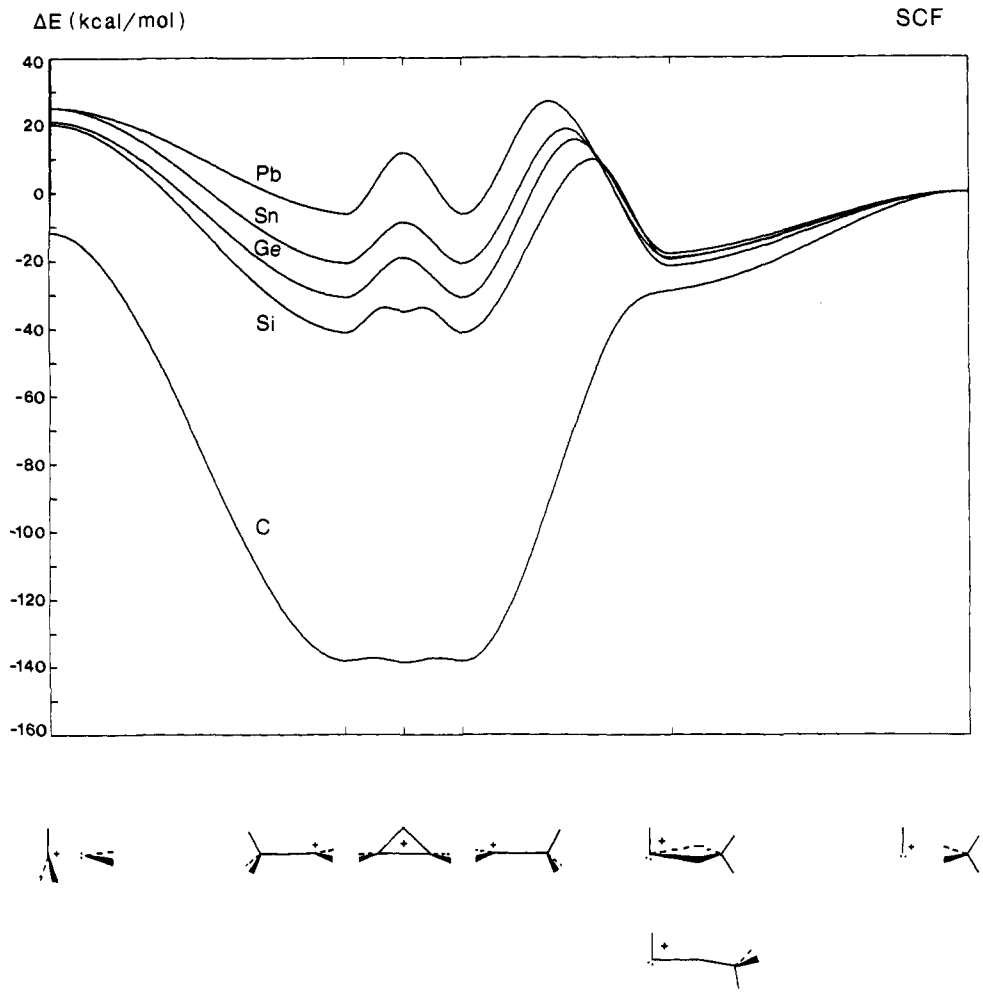

Figure 4. Schematic view of the $X_2H_5^+$ potential surfaces with a common zero energy corresponding to the dissociated fragments $XH^+ + XH_4$. SCF level.

schematize the various relevant cross sections in the hypersurfaces along a single coordinate. At each end of the coordinate, we locate the natural dissociation asymptotes from the two main isomers, namely the sets $XH_3^+ + XH_2(^1A_1)$ for the classical form and $XH^+(^1\Sigma^+) + XH_4$ for the bridged forms. Our walk along the potential surface will correspond to the events depicted in **21**, with

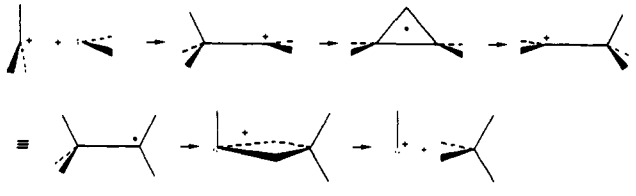

21

the right-hand side asymptote dissociating the double bridge. For clarity, we shall skip the single bridge step since this form is close, both in structure and energy, to the doubly bridged one. The building blocks of the double bridges are chosen to have the zero relative energy that will be common to all the surfaces, as we did for the neutral systems. The various energy curves are drawn in Figure 4 for the SCF energies and Figure 5 for the MP4 energies. These schemes provide a global and synthetic view of each potential surface and make comparison easier within group 14. Comparison of Figures 4 and 5 illustrates the main effects of electronic correlation on the shape of these surfaces, namely, (1) annihilation of minima (for carbon), (2) tempering of the barriers and, to a lesser extent, of the energy differences between the minima, and (3) enhancement of the energy required for dissociation into fragments. Let us now focus on Figure 5 that should picture the real physical potential surfaces. As we can expect, carbon behaves in a singular way with a single deep well located far below the building fragments. The heavier elements exhibit flatter surfaces whose minima are less far from the separated fragments. Comparison with the curves for neutral X_2H_4 exhibits the same trends.[11] Again, a striking feature is that the energy gained from the formation of an electron-deficient double bridge from two isolated fragments is rather constant with whatever atom (except carbon, here) as illustrated by the bundle of curves in the right-hand part of Figures 4 and 5. Furthermore, this binding energy is about the same (≈30 kcal/mol) in the present case where the electron-deficient double bridge is built from two different fragments and in the case of X_2H_4 where the fragments were identical. This is in agreement with recent results on the separability of the bridges in such systems,[23] but one may also see in it a balance between two opposite effects. The partially intermolecular nature of the link, that should induce a weak binding energy, is compensated by the cationic nature of the fragment that receives the two electron pairs of the double bridge.

Both Table III and Figures 4 and 5 indicate that carbon is again singular in that it does not favor the set $XH^+ + XH_4$ relative to the set $XH_3^+ + XH_2$, unlike the other elements. The disproportionation reaction

$$XH_3^+ + :XH_2 \rightarrow :XH^+ + XH_4 \qquad (1)$$

involves two hydrogen transfers which can be made from the full

(22) Trinquier, G.; Barthelat, J.-C. *J. Am. Chem. Soc.* **1990**, *112*, 9121.

(23) (a) Trinquier, G.; Garcia-Cuesta, I.; Malrieu, J.-P. *J. Am. Chem. Soc.* **1991**, *113*, 6465. (b) Trinquier, G.; Malrieu, J.-P. *J. Am. Chem. Soc.* **1991**, *113*, 8634.

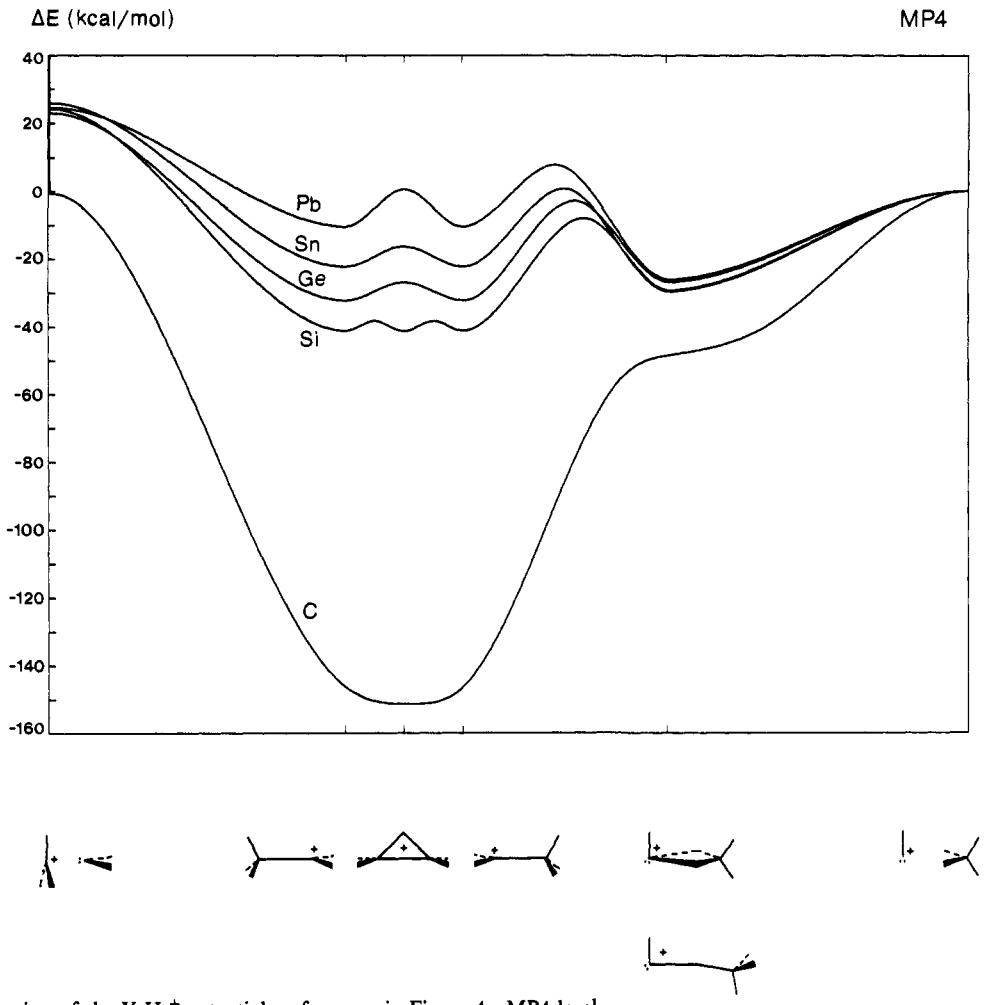

Figure 5. Schematic view of the $X_2H_5^+$ potential surfaces, as in Figure 4. MP4 level.

pathway **21**. The energy changes associated with this pathway are therefore the differences between the two asymptotes in Figures 4 and 5. These reaction energies are calculated as follows (in kcal/mol):

	SCF	MP4
C	+12	+1
Si	-20	-24
Ge	-21	-23
Sn	-25	-26
Pb	-25	-25

To rationalize and understand these numbers, let us see reaction 1 as the neutral disproportionation 2

$$2XH_2(^1A_1) \longrightarrow X(^3P) + XH_4 \quad (2)$$

$$\downarrow H^+ \qquad \downarrow H^+$$

$$XH_3^+ + XH_2 \longrightarrow XH^+ + XH_4 \quad (1)$$

followed by the single protonation where available in each member (XH_2 in the left member, X in the right member). The energy for reaction 1 is that of the neutral disproportionation 2 corrected by the *differential* proton affinity of $XH_2(^1A_1)$ and $X(^3P)$. These quantities, calculated at the SCF level, are plotted in Figure 6. The bottom curve figures the energy change in 2, which is also the differential X–H bond energy in XH_2 and XH4 (weighted by a factor of 4). Reaction 2 is exothermic, especially with carbon for which CH_4 is strongly favored. As expected from the known relative preference for divalent forms with heavier elements, the energy gain in reaction 2 is less and less important, and the corresponding curve in Figure 6 rises close to zero. The proton affinity of XH_2 is much larger than that of X for carbon. For

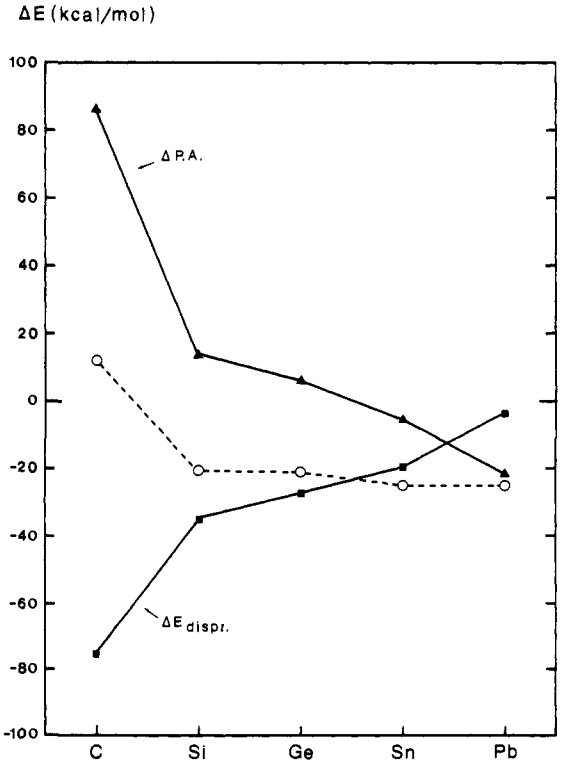

Figure 6. SCF-calculated energy for the exchange reaction $XH_3^+ + XH_2 \rightarrow XH^+ + XH_4$ (dashed line), as resulting from the sum of the disproportionation reaction $2XH_2(^1A_1) \rightarrow X(^3P) + XH_4$ (bottom curve) and the differential proton affinity $PA(XH_2)$–$PA(X)$ (top curve).

silicon and germanium, the difference vanishes, and for tin and lead the trend is reversed. The corresponding differential proton affinity curve therefore drops from carbon to lead and crosses the zero-energy axis (top curve in Figure 6). Such a trend originates in the decreasing availability of the lone pair in singlet XH_2.[24] The proton affinity of XH_2 is smaller with heavier atoms because the lone pair has more and more s character and the s–p mixing is less and less favored as one goes down group 14.[25] The proton affinity for $X(^3P)$ is larger with heavier atoms, but, whereas the difference is moderate from silicon to lead (9 kcal/mol), it is quite prominent from carbon to silicon (55 kcal/mol).[26] The resulting energy for reaction 1 is given by the algebraic sum of the two curves in Figure 6, yielding the dashed line in the same figure. From silicon to lead, neutral disproportionation prevails over the differential proton affinities. Since the two curves have a nearly symmetrical shape, the energy for reaction 1 is negative and rather constant around −20–25 kcal/mol. For carbon, the differential proton affinity prevails, and reaction 1 is no longer favored. Finally, note that correlation effects significantly alter this reaction energy for carbon, while being less and less effective when going down to heavier elements. Although reaction 1 is isodesmic, the character of the lone pair on $:XH_2$ may be different from that on $:XH^+$. For heavy elements, both lone pairs have a strong s character. For carbon, the lone pair in singlet $:CH_2$ has more s–p mixing than that in singlet $:CH^+$, therefore bringing less correlation energy to the left-side member of eq 1 than to the right-side member and consequently decreasing the endothermicity of the reaction. To a lesser extent, the same phenomenon will increase—but less and less—the exothermicity for the following atoms.

The energy differences between the two asymptotic sets of fragments can therefore be traced to atomic characteristics. The relative energies are in all cases smaller than those obtained when making $X_2H_5^+$ from the set $XH_3^+ + XH_2$. If one extracts from Table IV the energy brought by the coupling of XH_3^+ and XH_2 into the classical form, **12**, one gets another measure of the availability of the lone pair in singlet $:XH_2$. The following corresponding energies (in kcal/mol) reflect, among other things, the gap between the second period and the next ones and the regularly increasing inertia of the lone pair on XH_2:

	SCF	MP4
C	126	143
Si	61	65
Ge	52	55
Sn	46	48
Pb	31	35

The proton affinities for the most stable forms of X_2H_4 can be obtained from the energies listed on top of Table IV. For ethylene and disilene, our MP4 results are in agreement with the CEPA calculations by Köhler and Lischka.[5] For estimating the proton affinities, the zero-point vibrational energy differences between X_2H_4 and $X_2H_5^+$ must now be taken into account since they are no longer negligible. These corrections decrease the MP4 energy differences by 5–6 kcal/mol, which leads to the following best estimates for the proton affinities at 0 K:

C_2H_4	166 kcal/mol
Si_2H_4	203
Ge_2H_4	202
Sn_2H_4	200
Pb_2H_4	185

For C_2H_4 and Si_2H_4, the proton affinities at 298 K were deduced from experimental measurements at 163[27] and 200 kcal/mol,[8] respectively. Our values are in reasonable agreement for these two cases, although the G2 theoretical procedure leads, for Si_2H_4, to an even better agreement (200 kcal/mol at 0 K, 201 kcal/mol at 298 K).[7] We predict roughly similar values for Si_2H_4, Ge_2H_4, and Sn_2H_4 and a smaller value for Pb_2H_4.

Toward Structural Prediction from Simple Rules

This work has indicated the various structural possibilities for group 14 heavier analogues of the ethyl cation. Beyond the single deep well characterizing $C_2H_5^+$, there appears competing bridged structures which become the preferred arrangements for the heaviest cations $Sn_2H_5^+$ and $Pb_2H_5^+$. As in the case of X_2H_4, the potential surface is more broken up with heavy atoms than with carbon. Unlike the neutral case where Sn_2H_4 had the largest number of minima (five),[11] here, $Si_2H_5^+$ has the largest number of minima (four). The formation of a double bridge by two electron-deficient bonds seems to be a process with a fairly constant binding energy, whatever the atom and the fragments ($2XH_2$ for X_2H_4, $XH^+ + XH_4$ for $X_2H_5^+$). Such a structure is therefore always a potential atomic arrangement. The relative energies of the competing isomers (depending on their internal binding energies) will determine if this minimum can exist as such or will be caught in the well of another isomer. One can go a step farther and try to rationalize the relative thermodynamic stabilities of the isomers.

The competition between **1** and **2** involves an interplay between the nature and energy of the XX bonds and atomic characteristics. We have explained above why **1** collapses into **2** for carbon. The reason why **2** collapses into **1** for the heavier elements can be related, basically, to the arguments accounting for the occurrence of nonclassical distortions at the corresponding neutral double bonds (see **10**). Existence conditions have been devised, related to the X=X bond energy and to the singlet–triplet splittings of the fragments the XX bond is built from.[28,29] Can we assess, in the same way, the relative stabilities of **1** and **3** from simple bond-energy arguments?

The classical form **1** is bound by five X–H bonds and one X–X bond. The doubly bridged form **3** is tied by three X–H bonds and two X–H–X bridges. As discussed above, the bond energy for each X–H–X bridge in **3** is about equal to that of the X–H bond augmented by a constant amount of—say—15–20 kcal/mol that we shall call BBB, standing for *bridge bonding benefit*. The bond-energy count now becomes as follows.

1: 5XH + XX

3: 3XH + 2XHX = 5XH + 2BBB

The relative stability of **1** and **3** will therefore roughly depend on the balance between the XX bond energy and twice the BBB increment. Taking 2BBB = 30 kcal/mol does not seem sufficient to account for the preference of **3** over **1** with tin and lead. By taking 2BBB ≈ 40 kcal/mol and the following values for the X–X bond energies (in kcal/mol)[30]

C	83
Si	54
Ge	45
Sn	36
Pb	33

(24) The proton affinities for $^1A_1$ XH_2 are calculated as follows (in kcal/mol):

	SCF	MP4
C	223	220
Si	206	204
Ge	198	194
Sn	194	193
Pb	179	179

(25) This effect mainly originates in the increasing mismatch of the mean radii of the s and p atomic orbitals: Kutzelnigg, W. *Angew. Chem., Int. Ed. Engl.* **1984**, *23*, 272.

(26) This effect can be traced to the atomic $^3P \rightarrow {}^1D$ and $^3P \rightarrow {}^1S$ separations since these atomic states (mainly the ^1S one) are involved in the $^1\Sigma^+$ molecular state of the XH^+ diatom. The corresponding transitions require 29 and 62 kcal/mol, respectively, for carbon, but only 18 and 44 kcal/mol, respectively, for silicon: Moore, C. E. *Atomic Energy Levels*, N.B.S., Washington, DC, 1949.

(27) Lias, S. G.; Liebman, J. F.; Lievin, R. D. *J. Phys. Chem. Ref. Data* **1984**, *13*, 784.

(28) Trinquier, G.; Malrieu, J.-P. *J. Am. Chem. Soc.* **1987**, *109*, 5303.

(29) Malrieu, J.-P.; Trinquier, G. *J. Am. Chem. Soc.* **1989**, *111*, 5916.

(30) From Purcell, K. F.; Kotz, J.-C. *Inorganic Chemistry*; Saunders: Philadelphia, PA, 1977; p 270. For lead, the value is taken from the following: Harrison, P. G. In *Comprehensive Organometallic Chemistry*; Wilkinson, G. et al., Eds.; Pergamon Press: Oxford, 1983; Vol. 2, p 629.

we can now account for the reversal of relative stability between germanium (**1** < **3** by 6 kcal/mol) and tin (**3** < **1** by 7 kcal/mol). Interestingly, this also accounts for the relative stabilities of the corresponding neutral analogues **22** and **23** for X_2H_4 (Ge, **22** < **23**; Sn, **23** < **22**, by 7 kcal/mol in both cases)[11] where there are 4XH + XX in **22** and 2XH + 2XHX = 4XH + 2BBB in **23**, so

22 **23**

that the problem again reduces to a balance between an X–X bond energy and a constant increment of 2BBB. This reduction can also be applied to some systems with atoms from other groups, such as the two X_2H_2 isomers **24** and **25** of group 13. From boron

24 **25**

to aluminum, structure **25** becomes more stable than **24**,[31] which corresponds to the expectedly weaker X–X bond energies beyond boron in group 13.[32] The model also favors **26** over **27** for B_2H_4 and the opposite with the heavier analogs. Since there is enough

26 **27**

room, a triply bridged form, **28**, is also possible. Assuming again that the bridges are independent, this arrangement is granted an increment of 3BBB, larger than that in **27** (2BBB) and therefore awarded a larger thermodynamic stability. These trends are confirmed by ab initio calculations.[33]

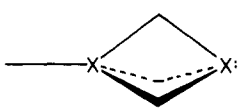

28

It must be kept in mind that the competition X–X bond versus X–H–X bridge only makes sense if (1) there is enough room (i.e., vacant orbitals) for making the bridges, and (2) there are enough electrons to make the X–X bond. This is why neither ethane C_2H_6 nor diborane B_2H_6 are relevant in the competition, since they do not meet conditions (1) and (2), respectively.

Beyond the present results on the $X_2H_5^+$ cations, we may therefore propose simple and naive ways to set up the structural diversity and estimate structural preferences. It is true that "the first row of the periodic table is unique and, hence, not always a good model for predicting the chemistry of subsequent rows",[13] but simple ratios, characteristic of given atoms, and given fragments may now help us to formulate preliminary ideas of the isomeric preferences in main group chemistry. The case of unsaturated hydrides is illustrated in Table VI, using two such ratios. These ideas should be extended to more general systems such as the fluorine bridges. In these compounds, the energy increment for bridge bonding (here three-center four-electron bridges) varies widely[22] and the basically ionic nature of the bonds could lead to additional rules based on pure electrostatic arguments. To understand, remember and predict structural trends, the main-group chemist disposes of simple and efficient tools, often based on electron counting, such as the octet rule, the $4n + 2$ rule, the VSEPR model, or Wade's rules. Although the present model needs to be further refined and checked,[34] time may come, soon, to add it to the list of such predictive tools.

In summary, we have shown in this work the existence of other structures for $X_2H_5^+$: the singly and doubly bridged complexes $XH^+ + XH_4$. These arrangements are local minima with all group 14 atoms except carbon and the doubly bridged form is the preferred isomer for tin and lead. Once more, the carbon-containing system has a single deep minimum on the potential surface, while the heavier analogues have several competing local minima. The confirmed general propensity to polybridged arrangements in heavy-atom-containing hydrides can finally be roughly accounted for through simple bond-energy systematics. The structural behavior for the mixed cations XYH_5^+ should be deducible from the present homopolar results. Nonobvious cases are those where a carbon atom is involved. Even in such cases, however, bond-energy arguments may be used, as illustrated for $CSiH_5^+$. Since the C–H bond energy is higher than that of Si–H (99 vs 76 kcal/mol),[30] the methylsilyl cation $H_3C–SiH_2^+$ is expected to be favored over the silylmethyl cation $H_3Si–CH_2^+$, which is well-confirmed by the theoretical exploration of the corresponding potential surface.[35]

Acknowledgment. The author thanks J.-P. Daudey, J.-P. Malrieu, and G. Trēboux for stimulating discussions. The Laboratoire de Physique Quantique is part of the IRSAMC institute.

Appendix

All the calculations were performed with the HONDO8 program available from the MOTECC package.[36] For all group 14 atoms, effective core potentials were used.[37] For tin and lead atoms, these take into account mean relativistic effects, described through the mass-velocity and Darwin terms.[38] The valence basis sets, which consist in four Gaussian functions per orbital, contracted to the double-ζ level, were optimized on the ^3P ground state of the atom using the corresponding effective core potentials. To these orbitals, a d polarization function is added with exponents 0.80 (C), 0.45 (Si), 0.25 (Ge), 0.20 (Sn), and 0.15 (Pb). A p polarization function is also added to the double-ζ basis set of hydrogen with an exponent of 0.80. The valence basis sets for all atoms are therefore of double-ζ plus polarization (DZP) type. Geometries are optimized at the SCF level with the gradient technique of the program (quasi Newton method). The final gradient components are generally better than 10^{-5} or 10^{-6} according to the case. The vibrational frequencies are obtained from force constants calculated by finite differences of analytical first derivatives (step size, 0.01 a.u., single differencing point). On each stationary point, electron correlation correction to the energy is calculated by means of the Möller–Plesset perturbation theory applied to the fourth order (MP4). For some of the structures

(31) Trēboux, G.; Barthelat, J.-C. Private communication.

(32) The mean bond energy for B–B is generally taken to be around 72 kcal/mol (ref 30). Further data are still lacking for the other group 13 atoms.

(33) (a) B_2H_4: Curtiss, L. A.; Pople, J. A. *J. Chem. Phys.* **1989**, *90*, 4314. Ruscic, B.; Schwarz, M.; Berkowitz, J. *J. Chem. Phys.* **1989**, *90*, 4576. Slanina, Z. *J. Phys. Chem.* **1991**, *95*, 1089. (b) Al_2H_4: Lammertsma, K.; Güner, O. F.; Drewes, R. M.; Reed, A. E.; Schleyer, P. v. R. *Inorg. Chem.* **1989**, *28*, 313. (c) Ga_2H_4: see ref 12. (d) $BAlH_4$: Mains, G. J.; Bock, C. W.; Trachtman, M.; Finley, J.; McNamara, K.; Fisher, M.; Wociki, L. *J. Phys. Chem.* **1990**, *94*, 6996. (e) $BGaH_4$ and $AlGaH_4$: see ref 13.

(34) Accurate values for the bond energy increments E_σ and $E_{\sigma+\pi}$ are needed as well as fragment ΔE_{ST} and BBB increments. We believe that the bridge bonding increment is not constant in general, even for the symmetrical electron-deficient double bridges (see section V in ref 23b). In group 13 XYH_6, the 2BBB increment is calculated at 29–41 kcal/mol according to the nature of the atoms (B, Al, Ga) and the level of calculation (see ref 33d and the following: McKee, M. *J. Phys. Chem.* **1990**, *94*, 435; **1991**, *95*, 6519. Mains, G. J.; Bock, C. W.; Trachtman, M. *J. Phys. Chem.* **1990**, *94*, 5449. Lammertsma, K.; Leszcynski, J. *J. Phys. Chem.* **1990**, *94*, 2806. McKee, M. L. *Chem. Phys. Lett.* **1991**, *183*, 510.). A value of ≈15–20 kcal/mol for the BBB increment seems to be sound.

(35) Pople, J. A.; Apeloig, Y.; Schleyer, P. v. R. *Chem. Phys. Lett.* **1982**, *85*, 489.

(36) Dupuis, M. MOTECC89, IBM Corporation, Kingston, NY.

(37) Durand, Ph.; Barthelat, J.-C. *Theor. Chim. Acta* **1975**, *38*, 283.

(38) Barthelat, J.-C.; Pēlissier, M.; Durand, Ph. *Phys. Rev. A* **1981**, *21*, 1773.

1 and 2, CASSCF multiconfigurational calculations were performed with active spaces of three orbitals and two electrons. For the singly bridged structures 2, the corresponding multiconfigurational wave function involves four configurations. The energy lowering brought by the CASSCF procedure with respect to the SCF energy represents the intrapair correlation energy of the X-H-X two-electron bridge in 2. It is calculated at 16.3 kcal/mol in $C_2H_5^+$, 13.6 kcal/mol in $Si_2H_5^+$, and 14.4 kcal/mol in $Pb_2H_5^+$. Similar valence correlation energies were obtained in the corresponding neutral or dicationic singly or doubly bridged systems.[11,23] For the classical form 1 of $Si_2H_5^+$, such an active space keeps localized on the Si_1-H_1 region, and the CASSCF extra energy (12.1 kcal/mol) now corresponds to the correlation energy of this Si-H bond.

Ab Initio Calculations on the Lower Excited States of Short-Chain Polyenals

Marianne Ros,[†] Edgar J. J. Groenen,*[,†] and Marc C. van Hemert[‡]

Contribution from the Centre for the Study of Excited States of Molecules, Huygens Laboratory, P.O. Box 9504, and Department of Chemistry, Gorlaeus Laboratories, P.O. Box 9502, University of Leiden, 2300 RA Leiden, The Netherlands. *Received January 21, 1992*

Abstract: The lower excited states of the planar all-trans isomers of crotonaldehyde, hexadienal, and octatrienal have been investigated by multi-reference single and double excitation configuration interaction (MRD-CI) calculations. For crotonaldehyde we find both the lowest excited singlet state S_1 and the lowest triplet state T_0 to be $n\pi^*$ in nature; for hexadienal and octatrienal S_1 is $n\pi^*$ and T_0 is $\pi\pi^*$ in nature. Bond-order reversal stabilizes the lower excited states and destabilizes the ground state. The $\pi\pi^*$ states decrease more in energy than the $n\pi^*$ states upon lengthening the polyenal. We calculate the radiative lifetime of the $^3\pi\pi^*$ state in the ground-state geometry to vary from 35 ms for crotonaldehyde to 75 s for octatrienal and explain the absence of phosphorescence for polyenals.

1. Introduction

The low-lying excited states of linear conjugated molecules continue to attract attention from spectroscopists and theoreticians because of the role played by such compounds in photochemical processes as photoisomerization and photoconductivity. These chromophores are much more difficult to understand than one would judge from their simple composition, and even the quantum-chemical description of relatively short chains presents significant problems. Here we report on ab initio calculations for three polyenals $CH_3(—CH=CH)_n—CHO$: *trans*-crotonaldehyde (CA, $n = 1$), *all-trans*-hexadienal (HD, $n = 2$), and *all-trans*-octatrienal (OT, $n = 3$).

Experimental observations on polyenals largely concern their excited singlet states. Birge et al. studied the vapor-phase absorption spectra for CA in the wavelength region corresponding to the excitation into the first $^1n\pi^*$ state.[1] These authors concluded that in this state CA is approximately planar and that considerable bond-order reversal takes place, i.e. double bonds become longer and single bonds become shorter upon excitation. Das and Becker recorded absorption and emission spectra for a series of unsubstituted polyenals in order to determine the singlet-state ordering as a function of chain length.[2] For $n \leq 3$ they concluded the lowest excited singlet state to be $n\pi^*$ in nature.

Polyenals do not phosphoresce, which severely hinders the investigation of their lowest triplet state. From singlet-triplet absorption spectra Birge et al. assigned for CA the lowest triplet state to be of $n\pi^*$ character.[3] These authors asserted that, as for the $^1n\pi^*$ state, CA in the $^3n\pi^*$ state is planar and the bond orders are reversed. On the other hand, from time-resolved EPR spectra Yamauchi et al.[4] claimed the relaxed lowest triplet state of CA to be of $\pi\pi^*$ character and the molecule to twist severely about the ethylenic bond upon triplet excitation. Evans determined the location of the lowest triplet state of polyenals with $n = 3$, 4, and 5 by recording $S_0 \rightarrow T_0$ absorption spectra in the presence of high-pressure oxygen.[5] Recently, Ros et al. identified by electron-spin-echo (ESE) spectroscopy the lowest triplet state of polyenals with $n = 2$, 3, 4, and 5 as a $\pi\pi^*$ state and concluded that these molecules are planar in T_0.[6]

Theoretical chemical studies of polyenals are scarce. To the best of our knowledge calculations of all-trans isomers of polyenals have not been carried out with ab initio methods so far. For CA Birge et al.[3] and Boerth[7] performed CNDO/II and INDOUV calculations, respectively, in order to determine the energy of the lower excited singlet and triplet states. For polyenals that lack the terminal methyl group Inuzuka and Becker calculated excited-state energies within the framework of PPP-SCF-MO-CI.[8] They found the lowest triplet state for $n > 1$ to be $\pi\pi^*$ and the lowest excited singlet state for $n < 4$ to be $n\pi^*$. According to their calculations the energy of the $n\pi^*$ states remained constant and that of the $\pi\pi^*$ states decreased upon increasing the chain length.

As far as $\pi\pi^*$ states are concerned we can relate the description of polyenals to that of polyenes, linear conjugated chains without the aldehyde group. Lack of intersystem crossing for polyenes has severely precluded the investigation of their triplet-state properties. Regarding the singlets, a major advance in understanding was made by the discovery of a low-lying excited singlet state of A_g character, to which the transition from S_0 is electric-dipole forbidden.[9] An adequate theoretical description of this state requires a proper inclusion of electron correlation. The singlet-state ordering is only correctly reproduced by a configu-

[†] Huygens Laboratory.
[‡] Gorlaeus Laboratories.

(1) Birge, R. R.; Pringle, W. C.; Leermakers, P. A. *J. Am. Chem. Soc.* **1971**, *93*, 6715.
(2) Das, P. K.; Becker, R. S. *J. Phys. Chem.* **1982**, *86*, 921.
(3) Birge, R. R.; Leermakers, P. A. *J. Am. Chem. Soc.* **1972**, *94*, 8105.
(4) Yamauchi, S.; Hirota, N.; Higuchi, J. *J. Phys. Chem.* **1988**, *92*, 2129.
(5) Evans, D. F. *J. Chem. Soc.* **1960**, 1735.
(6) Ros, M.; Groenen, E. J. J. *Chem. Phys. Lett.* **1989**, *154*, 29. Ros, M.; Groenen, E. J. J. *J. Chem. Phys.* **1991**, *94*, 7640.
(7) Boerth, D. W. *J. Org. Chem.* **1982**, *47*, 4085.
(8) Inuzuka, K.; Becker, R. S. *Bull. Chem. Soc. Jpn.* **1972**, *45*, 1557. Inuzuka, K.; Becker, R. S. *Bull. Chem. Soc. Jpn.* **1974**, *47*, 88.
(9) Hudson, B. S.; Kohler, B. E.; Schulten, K. In *Excited States*; Lim, E. C., Ed.; Academic Press: New York, 1982; Vol. 6, p 1.

0002-7863/92/1514-6820$03.00/0